17.2, 14.3, 12.6; HRMS calcd for $C_{53}H_{93}NO_{12}Si_2Na$ (M + Na) 1014.613, found (FAB) 1014.610.

506BD (1). To a solution of the tricarbonyl described above (18.3 mg, 18.3 mmol) in 1 mL of acetonitrile was added 1 mL of a 48% solution of HF in acetonitrile. After 1 h the reaction was quenched by adding the reaction mixture to a stirring, biphasic mixture of ether (10 mL) and saturated aqueous $NaHCO_3$ (10 mL). The ether layer was washed with three additional portions of $NaHCO_3$, dried over $MgSO_4$, filtered, and concentrated. Flash chromatography (70% EtOAc in hexane) gave 8 mg of a mixture of **1** and the seven-membered ring hemiacetal isomer (resulting from cyclization of the secondary alcohol onto the C9 ketone, hereafter referred to as **iso-1**) enriched in **1** as well as 4 mg of a mixture enriched in **iso-1**. The hemiacetal isomers were separated by HPLC on a 10 mm × 25 cm silica gel column (2-mg portions, 5.0 mL/min, 254-nm wavelength detector, 40% EtOAc in hexane) to give 5 mg of pure **1** (retention time = 7.2 min) and 2.5 mg of pure **iso-1** (retention time = 9.6 min). Data for **1**: $[\alpha]^{23}_D$ -45.8° (*c* 0.085, $CHCl_3$); IR (film) 3480 (br), 2930, 2856, 1734, 1716, 1651, 1633, 1456, 1269, 1230, 1095; ^{1}H NMR (500 MHz, $CDCl_3$) δ 6.84-6.81 [6.96-6.91] (d, *J* = 16.1, 1 H, C20), 5.61-5.58 [5.78-5.75] (d, *J* = 16.1, 1 H, C19), 5.39 (s, 1 H, OH of hemiacetal), 5.15-5.12 [5.19] (dd, *J* = 10.1, 4.1, 1 H, C16), 5.13 [5.21] (s, 1 H, C2), 5.04 (d, *J* = 9.2, 1 H, C24), 4.82 (s, 1 H, C22), 4.52-4.49 [3.65] (d, *J* = 13.2, 1 H, C6), 4.09-4.07 (dd, *J* = 9.5, 1.3, 1 H, C14), 3.69 (dd, *J* = 3.0, 1.4, 1 H, C15), 3.45-3.30 (mult, 2 H, C13, C27), 3.37 (s, 3 H), 3.36 (s, 3 H), 3.35 (s, 3 H), 2.97-2.92 (mult, 1 H, C28), 2.86-2.81 (t, *J* = 13.6, 1 H, C6), 2.39-2.16 (mult, 2 H), 2.15-2.06 (mult, 2 H), 2.05-1.99 (mult, 1 H), 1.98-1.88 (mult, 1 H), 1.82-1.65 (mult, 2 H), 1.61 (s, 3 H), 1.58-1.53 (mult, 1 H), 1.42-1.52 (mult, 2 H), 1.41-1.26 (mult, 2 H), 1.25-1.02 (mult, 4 H), 1.1 (s, 3 H), 1.0 (s, 3 H), 0.97 (d, *J* = 6.7, 3 H), 0.93-0.91 (mult, 6 H); ^{13}C NMR (75 MHz, $CDCl_3$) δ 169.8, 169.2, 166.5, 150.9, 135.7, 130.1, 129.9, 121.4, 98.6, 86.1, 84.3, 84.1, 75.9, 75.1, 75.0, 74.0, 73.5, 70.9, 58.1, 56.6, 56.4, 56.2, 41.1, 40.7, 40.2, 35.2, 34.3, 34.0, 33.5, 32.4, 31.2, 31.1, 30.2, 30.0, 29.7, 28.8, 26.8, 26.7, 24.4, 23.3, 20.6, 19.8, 18.9, 16.4, 15.5; HRMS calcd for $C_{38}H_{59}NO_{12}Na$ (M + Na) 744.393, found (FAB) 744.395. Data for **iso-1**: $[\alpha]^{23}_D$ -45.8° (*c* 0.085, $CHCl_3$); IR (film) 2930, 2856, 1728, 1709, 1633, 1456, 1269, 1230, 1095; ^{1}H NMR (500 MHz, $CDCl_3$) δ 7.12-7.08 (d, *J* = 16.1, 1 H, C20), 5.67-5.63 (d, *J* = 16.1, 1 H, C19), 5.22 (s, 1 H, OH of hemiacetal), 5.24-5.21 (dd, *J* = 2.2, 10.0, 1 H, C16), 5.10-5.07 (d, *J* = 9.9 Hz, 1 H, C24), 5.03 (s, 1 H, C22), 4.65-4.62 (d, *J* = 12.9, 1 H, C6), 3.49-3.47 (d, *J* = 9.9, 1 H, C14), 3.46-3.43 (d, *J* = 9.9, 1 H, C15), 3.36 (s, 3 H), 3.29 (s, 3 H), 3.28 (s, 3 H), 3.26-3.20 (mult, 1 H, C13), 3.19-3.09 (mult, 1 H, C6), 2.99-2.94 (mult, 1 H, C11), 2.88-2.83 (mult, 1 H, C27), 2.59 (s, 1 H), 2.3-1.89 (mult, 10 H), 1.73-1.61 (mult, 2 H), 1.52-0.72 (mult, 16 H), 1.38 (s, 3 H), 1.05 (s, 3 H), 0.94 (s, 3 H); ^{13}C NMR (75 MHz, $CDCl_3$) δ 211.2, 165.6, 152.9, 135.9, 129.9, 120.2, 98.7, 86.8, 84.0, 83.2, 78.1, 76.4, 74.8, 73.5, 59.1, 56.8, 56.5, 52.5, 44.1, 40.4, 40.2, 38.1, 35.1, 34.3, 31.1, 30.2, 29.7, 29.5, 27.2, 25.3, 22.9, 21.5, 19.7, 16.6, 15.6; HRMS calcd for $C_{38}H_{59}NO_{12}Na$ (M + Na) 744.393, found (FAB) 744.393.

Acknowledgment. We thank the NIGMS (GM-38627) for support of this research. A National Science Foundation Predoctoral Fellowship to T.J.W. and an American Cancer Society Fellowship to P.K.S. are gratefully acknowledged. We especially thank Professor Jon Clardy and Dr. G. D. Van Duyne for their important contributions to the FKBP ligand studies and for the X-ray structure determination of compound **8a**.

Note Added in Proof. The Ca^{2+}, calmodulin-dependent protein phosphatase calcineurin (PP2B) has recently been shown to be a common target of cyclophilin-CSA and FKBP-FK506 complexes in mammalian cells: Liu, J.; Farmer, J. D.; Lane, W. S.; Friedman, J.; Weissman, I.; Schreiber, S. L. *Cell* **1991**, *66*, 807-815.

Supplementary Material Available: Tables of crystal data, atomic coordinates, bond lengths and angles, and isotropic and anisotropic displacement coefficients (7 pages); tables of observed and calculated structure factors (5 pages). Ordering information is given on any current masthead page.

Secondary H/D Isotope Effects in Methyl-Transfer Reactions Decrease with Increasing Looseness of the Transition Structure

Saul Wolfe*,†,‡ and Chan-Kyung Kim†

Contribution from the Department of Chemistry, Queen's University, Kingston, Ontario, Canada K7L 3N6, and Department of Chemistry and Biochemistry, Simon Fraser University, Burnaby, British Columbia, Canada V5A 1S6. *Received July 23, 1990*

Abstract: The barriers of identity gas-phase methyl-transfer reactions $X^- + CH_3X \rightarrow XCH_3 + X^-$ are directly related to the looseness of their transition structures, and inversely related to the secondary kinetic isotope effects in the methyl group ($k_H/k_D < 1$). This means that the isotope effects decrease with increasing looseness of the transition structure, in contrast to current belief. Similar trends are observed at the 4-31G, 6-31+G*, and MP2/6-31+G* computational levels, and at each level, the C-H bond lengths of the transition structures do not depend upon X. The isotope effects are inverse primarily as a result of the increase in C-H (C-D) stretching frequencies (C-H (C-D) bond shortening) that accompanies the tetrahedral to trigonal change in geometry. Because of the constant C-H bond lengths in the transition structures, the largest isotope effect (smallest k_H/k_D) is seen with the substrate having the longest C-H bond. The contributions to the isotope effects from the complementary changes in the C-H (C-D) bending vibrations along the reaction coordinates are normal.

Introduction

There are interesting correlations between the energy changes along the reaction coordinates of S_N2 reactions, eq 1, and the changes in geometry that attend these reactions.[1] In the gas phase, the reaction coordinate is double-welled,[2] because of the presence of stable reactant and product ion-molecule complexes ($X^-\cdots CH_3Y$ and $XCH_3\cdots Y^-$).

$$X^- + CH_3Y \rightarrow XCH_3 + Y^- \quad (1)$$

For identity reactions (X = Y), ΔE^*, the central barrier computed at the 4-31G level[3] is linearly related to ΔE_{def}, the energy required

† Present address: Department of Chemistry, Simon Fraser University, Burnaby, BC, Canada V5A 1S6.

‡ Holder of a Canada Council Killam Research Fellowship, 1990-1992.

(1) (a) Mitchell, D. J.; Schlegel, H. B.; Shaik, S. S.; Wolfe, S. *Can. J. Chem.* **1985**, *63*, 1642. (b) Shaik, S. S.; Schlegel, H. B.; Wolfe, S. *J. Chem. Soc., Chem. Commun.* **1988**, 1322.

(2) Brauman, J. I.; Olmstead, W. N.; Lieder, C. A. *J. Am. Chem. Soc.* **1974**, *96*, 4030. Farneth, W. E.; Brauman, J. I. *Ibid.* **1976**, *98*, 7891. Olmstead, W. N.; Brauman, J. I. *Ibid.* **1977**, *99*, 4219.

(3) Mitchell, D. J. Ph.D. Thesis, Queen's University, Kingston, Ontario, 1981.

0002-7863/91/1513-8056$02.50/0

Table I. Calculated Energy Changes, Deformation Energies, and Transition-Structure Looseness in S_N2 Reactions $X^- + CH_3Y \rightarrow YCH_3 + Y^-$[a]

X, Y	ΔE_1	ΔE_2	ΔE^*	ΔH^*	ΔS^*	ΔG^*	ΔE_{def}	L^*
F, F	−12.50[b]	5.64[b]	18.54	18.14	−7.03	20.24	47.96	60.8
	−13.88[c]	−1.43[c]	12.45[c]	12.05[c]	−7.03	14.15[c]		
	−14.19[d]	−4.05[d]	10.14[d]	9.74[d]	−7.03	11.84[d]		
	−13.63[b,e]	−1.11[b,e]	12.93[e]	12.52[e]	−7.05[e]	14.63[e]	37.81[e]	52.6[e]
	−26.23[f]	−14.54[f]	11.69[f]	11.14	−5.42	12.76	40.8[f]	50.0[f]
Cl, Cl	−8.73[b]	6.28[b]	15.47	15.01	−9.73	19.91	39.78	62.9
	−9.44[c]	8.60[c]	18.04[c]	17.58[c]	−9.73	20.48[c]		
	−9.54[d]	6.55[d]	16.10[d]	15.64[d]	−9.73	18.54[d]		
	−9.50[b,e]	7.32[b,e]	17.34[e]	16.82[e]	−8.55[e]	19.37[e]	36.90[e]	56.1[e]
	−16.42[f]	−10.91[f]	5.51[f]	5.08	−5.55	6.73	28.9[f]	42.2[f]
FO, OF	−13.41[b]	13.67[b]	27.64	27.08	−5.75	28.80	49.45	67.2
	−22.08[f]	−3.21[f]	18.87[f]	17.98[f]	−0.07[f]	18.00[f]	41.15[f]	63.9[f]
CN, NC	−11.28[b]	20.30[b]	32.15	31.58	−10.35	34.67	57.85	81.3
	−13.44[c]	17.41[c]	30.84[c]	30.27[c]	−10.35	33.56[c]		
	−14.60[f]	13.92[f]	28.52[f]	27.80	−9.12	30.52	57.0[f]	79.5[f]
MeO, OMe	−8.86[b]	25.53[b]	35.28	34.39	−11.49	37.81	56.29	70.4
	−18.21[f]	11.95[f]	30.16[f]	28.86[f]	−3.77[f]	29.98[f]	48.2[f]	64.0[f]
NC, CN	−10.69[b]	35.57[b]	46.42	46.26	−12.75	50.06	67.09	89.8
	−11.52[c]	33.82[c]	45.34[c]	45.18[c]	−12.75	48.98[c]		
	−14.86[f]	28.90[f]	43.76[f]	43.41	−8.70	46.00	67.0[f]	89.2[f]
HCC, CCH	−5.07[b]	48.47[b]	53.53	53.54	−12.68	57.02	73.79	91.2
	−8.79[f]	41.63[f]	50.41[f]	50.05[f]	−12.20[f]	53.69[f]	73.48[f]	90.0[f]
F, Cl	−14.28[b]	−11.44[b]	2.99	2.83	−4.56	4.19	17.30	66.5
	−13.77[c]	−7.83[c]	5.94[c]	5.78[c]	−4.56	7.14[c]		
Cl, F	−7.75[b]	32.15[b]	41.16	39.89	−6.46	41.82	81.26	66.5
	−9.35[c]	18.86[c]	28.21[c]	26.94[c]	−6.46	28.87[c]		

[a] Energies are in kilocalories per mole from 6-31+G*-optimized structures, unless stated otherwise. Thermodynamic parameters refer to 298 K. [b] Zero-point energies have been taken into account. [c] From one-point MP2 calculations with the 6-31+G*-optimized structure. [d] From one-point MP4 calculations with the 6-31+G*-optimized structure. [e] Structures have been optimized at the MP2/6-31+G* level. [f] 4-31G data from ref 3.

to deform CH_3X from its geometry in the complex to its geometry in the transition structure,[1a] and also to L^*, eq 2, the percent

$$L^* = \%CX^* + \%CY^* \quad (2)$$

$$\%CX^* = 100(d^*_{CX} - d^0_{CX})/d^0_{CX}$$

$$\%CY^* = 100(d^*_{CY} - d^0_{CY})/d^0_{CY}$$

lengthening of the C–X and C–Y bonds during this process,[1b] where d^0 and d^* are the C–X (C–Y) bond lengths of CH_3X (CH_3Y) in the complexes and transition structures, respectively. For nonidentity reactions (X ≠ Y), there is an extended 4-31G linear correlation between the "looseness" of the transition structure and the sum of the forward and reverse central barriers.[1b] In these correlations, the deformation energy and looseness *increase* as the barriers increase, as predicted by the Shaik–Pross model of the S_N2 barrier.[4]

There is evidence that the looseness of an S_N2 transition structure is only marginally affected by solvation,[5] so that the trends just described are expected to persist in solution. One of the objectives of the present work is to reexamine the relationships between ΔE^* and ΔE_{def}, and between ΔE^* and L^*, at a higher computational level.[6] A second objective is to examine, in some detail, the magnitudes of the calculated secondary isotope effects (CH_3/CD_3) as a function of barrier height and looseness of the transition structure.

According to the theory of isotope effects,[7] a decrease in the force constants involving the light and heavy atoms along a reaction coordinate will lead to a normal kinetic isotope effect ($k_H/k_D > 1$). For the S_N2 mechanism, it is argued[8,9] that the secondary isotope effect k_{CH_3}/k_{CD_3} should be inverse, because the presence of entering and leaving groups in the transition state causes HCX bending force constants to *increase*, and the changes in these force constants make the dominant contribution to the isotope effect. A corollary of this argument[10] is that a decrease in the *magnitude* of k_{CH_3}/k_{CD_3} signals increased *tightening* of the transition state. In a seminal study, Schowen and his co-workers found k_H/k_D to be smaller in an enzymatic methyl-transfer reaction than in a related non-enzymatic reaction.[10] On the basis of the above reasoning, these researchers concluded that the enzyme causes a tightening of the transition state, and that this compression may represent the source of the enzymatic catalysis.

The most significant findings of the ab initio calculations reported here are that the behavior of the bending force constants and the variation in the magnitudes of the kinetic isotope effects as a function of transition state looseness are the opposite of those just discussed. The inverse kinetic isotope effect observed in a methyl-transfer reaction is caused mainly by the tightening of the C–H bonds[6b,11] (increased C–H stretching force constants) in response to the change in geometry from tetrahedral to trigonal. Bending force constants invariably *decrease* along the reaction coordinate, leading to normal contributions to the isotope effects.

Computational Methods

Geometries of separated reactants, ion–molecule complexes, and transition structures were optimized fully at the 4-31G,[3,12] 6-31+G*,[13] or MP2/6-31+G*[14] levels, using GAUSSIAN 86[15] or GAUSSIAN 90.[16] All

(4) Pross, A.; Shaik, S. S. *Acc. Chem. Res.* **1983**, *16*, 363. Shaik, S. S. *Prog. Phys. Org. Chem.* **1985**, *15*, 197. Shaik, S. S.; Schlegel, H. B.; Wolfe, S. *Theoretical Aspects of Physical Organic Chemistry*; Wiley: New York, in press.

(5) Westaway, K. C. *Can. J. Chem.* **1978**, *56*, 2691. Jorgensen, W. L.; Buckner, J. K. *J. Phys. Chem.* **1986**, *90*, 4651.

(6) (a) Tucker, S. C.; Truhlar, D. G. *J. Phys. Chem.* **1989**, *93*, 8138. (b) Tucker, S. C.; Truhlar, D. G. *J. Am. Chem. Soc.* **1990**, *112*, 3338. Zhao, X. G.; Tucker, S. C.; Truhlar, D. G. *J. Am. Chem. Soc.* **1991**, *113*, 826. (c) Shi, Z.; Boyd, R. J. *J. Am. Chem. Soc.* **1989**, *111*, 1575. *Ibid.* **1991**, *113*, 2434. (c) Vetter, R.; Zülicke, L. *J. Am. Chem. Soc.* **1990**, *112*, 5136.

(7) Wolfsberg, M.; Stern, M. J. *Pure. Appl. Chem.* **1964**, *8*, 225.

(8) Streitwieser, A., Jr.; Fahey, R. C. *Chem. Ind.* **1957**, 1417. Streitwieser, A., Jr.; Jagow, R. H.; Fahey, R. C.; Suzuki, S. *J. Am. Chem. Soc.* **1958**, *80*, 2326. Leffek, K. T.; Llewellyn, J. A.; Robertson, R. E. *Can. J. Chem.* **1960**, *38*, 1505. Wolfsberg, M.; Stern, M. J. *Pure Appl. Chem.* **1964**, *8*, 325.

(9) For recent reviews, see: Westaway, K. C. In *Isotopes in Organic Chemistry*; Buncel, E., Lee, C. C., Eds.; Elsevier: Amsterdam, 1987; Vol. 7, Chapter 5. McClennan, D. J. *Ibid.* Chapter 6.

(10) Mihel, I.; Knipe, J. O.; Coward, J. K.; Schowen, R. L. *J. Am. Chem. Soc.* **1979**, *101*, 4349. Gray, C. H.; Coward, J. K.; Schowen, K. B.; Schowen, R. L. *Ibid.* **1979**, *101*, 4351. Hegazi, M. F.; Borchardt, R. T.; Schowen, R. L. *Ibid.* **1979**, *101*, 4359. Rodgers, J.; Femec, D. A.; Schowen, R. L. *Ibid.* **1982**, *104*, 3263.

(11) Williams, I. H. *J. Am. Chem. Soc.* **1984**, *106*, 7206.

(12) Ditchfield, R.; Hehre, W. J.; Pople, J. A. *J. Chem. Phys.* **1971**, *54*, 724.

(13) Clark, T.; Chandrasekhar, J.; Spitznagel, G. W.; Schleyer, P. v. R. *J. Comput. Chem.* **1983**, *4*, 294.

Table II. Equilibrium Isotope Effects,[a] Kinetic Isotope Effects for the Central Barriers, Kinetic Isotope Effects from the Separated Reactants, and Their Stretching (S) and Bending (B) Components for S_N2 Reactions $X^- + CH_3Y$ (CD_3Y) → XCH_3 (XCD_3) + Y^-

	equilibrium K_{CH_3}/K_{CD_3}			central barrier k_{CH_3}/k_{CD_3}			separated reactants k_{CH_3}/k_{CD_3}		
X, Y	total	S	B	total	S	B	total	S	B
Cl, Cl	0.97[b]	0.92[b]	1.06[b]	0.97[b]	0.77[b]	1.25[b]	0.94[b]	0.71[b]	1.33[b]
	0.99[c]	0.87[c]	1.13[c]	0.99[c]	0.85[c]	1.16[c]	0.98[c]	0.75[c]	1.32[c]
	1.00[d]	0.93[d]	1.08[d]	0.97[d]	0.81[d]	1.20[d]	0.96[d]	0.75[d]	1.29[d]
F, F	0.99[b]	0.93[b]	1.08[b]	0.85[b]	0.80[b]	1.06[b]	0.84[b]	0.74[b]	1.14[b]
	1.03[c]	0.87[c]	1.18[c]	0.93[c]	0.89[c]	1.04[c]	0.95[c]	0.78[c]	1.23[c]
	1.01[d]	0.92[d]	1.11[d]	0.92[d]	0.89[d]	1.04[d]	0.93[d]	0.81[d]	1.15[d]
FO, OF	1.00[b]	1.05[b]	0.95[b]	0.81[b]	0.86[b]	0.94[b]	0.81[b]	0.91[b]	0.90[b]
	1.00[c]	1.03[c]	0.97[c]	0.88[c]	0.84[c]	1.05[c]	0.88[c]	0.87[c]	1.02[c]
CN, NC	0.99[b]	0.93[b]	1.06[b]	0.79[b]	0.75[b]	1.06[b]	0.78[b]	0.70[b]	1.12[b]
	0.99[c]	0.92[c]	1.08[c]	0.82[c]	0.75[c]	1.09[c]	0.81[c]	0.68[c]	1.18[c]
MeO, OMe	0.99[b]	1.05[b]	0.94[b]	0.80[b]	0.53[b]	1.51[b]	0.79[b]	0.56[b]	1.42[b]
	1.00[c]	0.71[c]	1.41[c]	0.85[c]	0.69[c]	1.22[c]	0.85[c]	0.49[c]	1.72[c]
NC, CN	1.03[b]	0.91[b]	1.08[b]	0.67[b]	0.79[b]	0.89[b]	0.69[b]	0.72[b]	0.96[b]
	1.03[c]	0.94[c]	1.10[c]	0.69[c]	0.76[c]	0.91[c]	0.71[c]	0.71[c]	1.00[c]
HCC, CCH	1.02[b]	0.95[b]	1.07[b]	0.66[b]	0.72[b]	0.93[b]	0.68[b]	0.68[b]	0.99[b]
	1.03[c]	0.93[c]	1.10[c]	0.63[c]	0.73[c]	0.95[c]	0.71[c]	0.68[c]	1.05[c]
F, Cl	0.97	0.86	1.13	0.91[b,e]	0.85[b]	1.07[b]	0.88	0.73	1.20
Cl, F	0.97	0.95	1.02	1.03[b,e]	0.77[b]	1.34[b]	1.00	0.73	1.37

[a] Refers to the reaction $X^- + CH_3Y \rightarrow (X^-\cdots CH_3Y)$, at 298 K. [b] From 6-31+G* calculations; frequencies have been scaled by 0.9. [c] From 4-31G calculations; frequencies have been scaled by 0.9. [d] From MP2/6-31+G* calculations; frequencies have been scaled by 0.9. [e] No transition state is observed at the 4-31G level, as predicted by Marcus theory.[20]

structures had either zero (reactants, ion–molecule complexes) or one (transition states) imaginary frequency. The frequencies were subjected to a standard[17] scaling of 0.9[18] for computation of the isotope effects.[19] In the GAUSSIAN 86 calculations, the frequencies of isotopically labeled species were obtained as described in ref 19. This protocol is available in GAUSSIAN 90; identical results are obtained by the two procedures.

Results and Discussion

Energies and Geometries. Table I summarizes the various energy quantities (ion–molecule well depths (ΔE_1), separated reactants → central barrier (ΔE_2, R → TS), ion–molecule complex → central barrier (ΔE^*, C → TS), ΔH^*, ΔS^*, ΔG^*, ΔE_{def}), as well as the L^* calculated for seven identity reactions (X, Y) = (F, F), (Cl, Cl), (MeO, OMe), FO, OF), (CN, NC), (HCC, CCH), and (NC, CN), and two nonidentity reactions (X, Y) = (F, Cl) and (Cl, F). The table contains the 6-31+G*//6-31+G* results, one-point energies calculated at MP2/6-31+G*//6-31+G*, MP2/6-31+G*//MP2/6-31+G* data for (X, Y) = (F, F) and (Cl, Cl), one-point energies calculated for (X, Y) = (F, F) and (Cl, Cl) at MP4/6-31+G*//6-31+G*, and the earlier 4-31G data.[1,3] The latter do not include (X, Y) = (F, Cl), because as predicted by Marcus theory,[20] no transition structure is observed at this computational level.

The energy changes for F/F and Cl/Cl are the most sensitive to basis set and correlation effects, but at the highest level examined (full optimization at MP2/6-31+G*), the results appear to agree with the most recent gas-phase experimental findings,[21] as already found by Tucker and Truhlar for Cl/Cl.[6a]

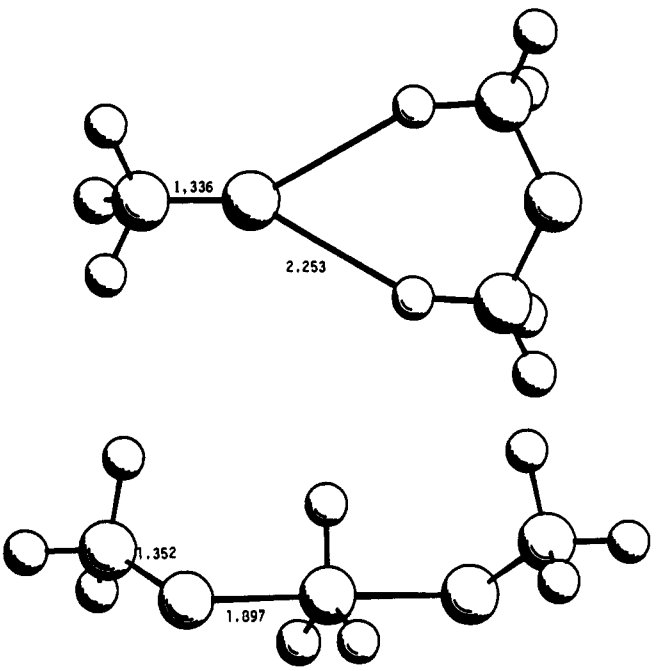

Figure 1. 6-31+G* structures of the $CH_3O^-\cdots CH_3$–OCH_3 ion–molecule complex (top) and the $(CH_3O$–CH_3–$OCH_3)^-$ transition state (bottom).

For the reaction $HO^- + CH_3OH$, only one genuine ion–molecule complex (no imaginary frequencies), corresponding to proton abstraction from *oxygen*, could be found at 6-31+G*//6-31+G*. Since this leads to ambiguity in the calculation of the S_N2 barrier, we also examined $CH_3O^- + CH_3OCH_3$. Only one ion–molecule complex was again found, with the interesting structure shown in Figure 1 (top); the transition structure (Figure 1, bottom) is normal.

Isotope Effects. Table II summarizes the H/D isotope effects computed at 4-31G and at 6-31+G*, for the equilibrium process ($IE_{R\rightarrow C}$), for passage over the central barrier ($IE_{C\rightarrow TS}$), and for the barrier from the separated reactants ($IE_{R\rightarrow TS}$). Also included are the MP2/6-31+G* isotope effects for (Cl, Cl) and (F, F). The k_H/k_D of 0.97 calculated for (Cl, Cl) at 6-31+G* and at MP2/6-31+G* is the same as that deduced by Albery and Kreevoy[22] and recently computed in the work of Truhlar.[6b] Since

(14) Pople, J. A.; Krishnan, R.; Schlegel, H. B.; Binkley, J. S. *Int. J. Quantum Chem., Symp.* **1979**, *13*, 325.
(15) Frisch, M. J.; Binkley, J. S.; Schlegel, H. B.; Raghavachari, K.; Melius, C. F.; Martin, R. L.; Stewart, J. J. P.; Bobrowicz, F. W.; Rohlfing, C. M.; Kahn, L. R.; Defrees, D. J.; Seeger, R.; Whiteside, R. A.; Fox, D. J.; Fluder, E. M.; Pople, J. A. *Gaussian 86*; Gaussian, Inc.: Pittsburgh, PA 15213.
(16) Frisch, M. J.; Head-Gordon, M.; Trucks, G. W.; Foresman, J. B.; Schlegel, H. B.; Raghavachari, K.; Robb, M. A.; Binkley, J. S.; Gonzalez, C.; Defrees, D. J.; Fox, D. J.; Whiteside, R. A.; Seeger, R.; Melius, C. F.; Baker, J.; Martin, R. L.; Kahn, L. R.; Stewart, J. J. P.; Topiol, S.; Pople, J. A. *Gaussian 90*; Gaussian, Inc.: Pittsburgh, PA, 1990.
(17) Pupyshev, V. I.; Panchenko, Y. N.; Bock, C. W.; Pongor, G. *J. Chem. Phys.* **1991**, *94*, 1247.
(18) Aljibury, A. L.; Snyder, R. G.; Strauss, H. L.; Raghavachari, K. *J. Chem. Phys.* **1986**, *84*, 6872.
(19) Wolfe, S.; Hoz, S.; Kim, C. K.; Yang, K. *J. Am. Chem. Soc.* **1990**, *112*, 4186.
(20) Wolfe, S. *Can. J. Chem.* **1984**, *62*, 1465.
(21) DePuy, C. H.; Gronert, S.; Mullin, A.; Bierbaum, V. M. *J. Am. Chem. Soc.* **1990**, *112*, 8650.
(22) Albery, W. J.; Kreevoy, M. M. *Adv. Phys. Org. Chem.* **1978**, *16*, 87.

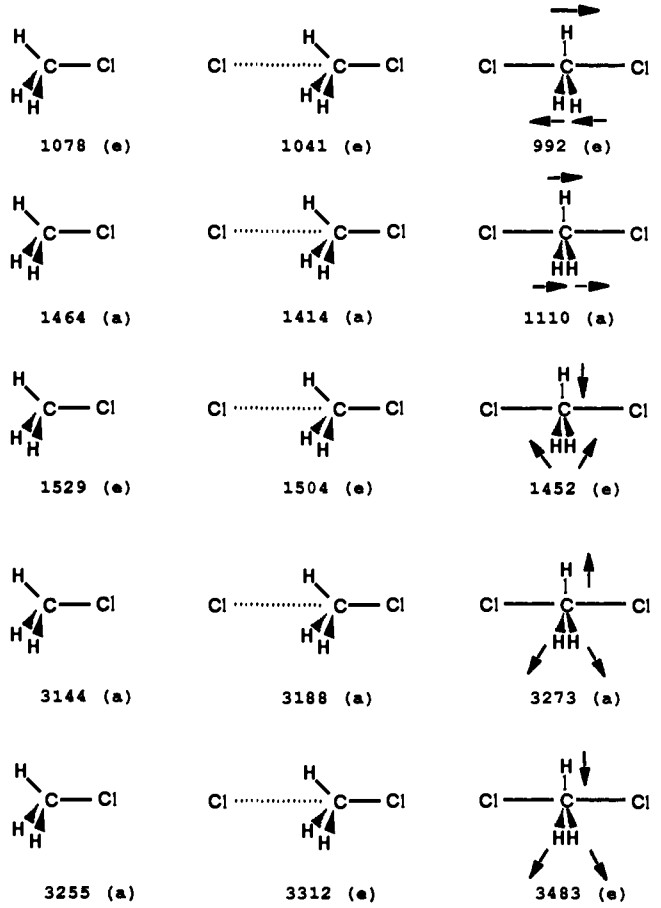

Figure 2. Unscaled C–H stretching and bending frequencies (cm^{-1}) computed at the MP2/6-31+G* level for CH_3Cl (left), the $Cl^-\cdots CH_3Cl$ ion–molecule complex (center), and the $(Cl–CH_3–Cl)^-$ transition state (right). The nature of the vibration in each case is indicated by the arrows superimposed on the transition structures.

$IE_{R\rightarrow TS} = IE_{C\rightarrow TS}IE_{R\rightarrow C}$,[11] and the equilibrium isotope effects are approximately constant and close to unity, the trends in $IE_{R\rightarrow TS}$ and in $IE_{C\rightarrow TS}$ are expected to be the same. Even a cursory inspection of Table II shows that this is the case and that, for the identity reactions, all kinetic isotope effects are inverse ($k_H/k_D < 1$).[23]

Analysis of individual frequencies allows these isotope effects to be partitioned into their stretching and bending components ($IE_T = IE_SIE_B$). Table II includes these data, and it can be seen that the bending components of the kinetic isotope effects tend to be normal. The overall isotope effects are therefore inverse because their stretching components are inverse. The reason for this is that in every case the C–H bond lengths decrease (and the stretching frequencies increase) with progress along the reaction coordinate. For example, in the reaction of chloride ion with methyl chloride, the MP2/6-31+G* C–H bond lengths are R, 1.0885; C, 1.0846; TS, 1.0724 Å and the (unscaled) symmetric stretching frequencies are R, 3144; C, 3188; TS, 3273 cm^{-1}.

MP2/6-31+G* Analysis of Cl^- + CH_3Cl. The complete set of MP2/6-31+G* C–H stretching and bending frequencies is summarized in Figure 2. It is noteworthy that all of the bending frequencies decrease with progress along the reaction coordinate, the largest change being observed for the inversion mode (the umbrella motion) of the methyl group.

The simplest rationalization of the C–H bond strengthening along the reaction coordinate is that this reflects the increasing s-character at carbon as its configuration changes from tetrahedral to trigonal. As summarized in Table III, at MP2/6-31+G* the C–H bond lengths calculated for CH_3Cl, CH_3^+, CH_3, and CH_3^- are, respectively, 1.0885, 1.0888, 1.0793, and 1.1009 Å; the corresponding (unscaled) symmetric stretching frequencies are, respectively, 3144, 3144, 3209, and 3010 cm^{-1}. These frequencies are not the same, so that cation-, radical-, and carbanion-forming tetrahedral → trigonal processes would be expected to proceed with unit, inverse ($k_H/k_D < 1$), and normal ($k_H/k_D > 1$) stretching isotope effects, respectively. The notion that the C–H bond lengths are responding to an $sp^3 \rightarrow sp^2$ change in hybridization would not be sufficient to account for the fact that charge development in the transition state also influences the isotope effects.[24]

Table III. MP2/6-31+G* C–H Stretching and Bending Vibrations of CH_3Cl, CH_3^+, CH_3, and CH_3^-

mode	nature	frequency (cm^{-1}) CH_3Cl[a]	CH_3^+[b]	CH_3[c]	CH_3^-[d]
e	CH_3 rock	1078			
a	CH_3 umbrella	1464	1462	482	819
e	CH_3 deformation	1529	1471	1470	1479
a	sym CH_3 stretch	3144	3144	3210	3011
e	antisym CH_3 stretch	3255	3357	3399	3118

[a] C–H = 1.0885 Å. [b] C–H = 1.0888 Å. [c] C–H = 1.0793 Å. [d] C–H = 1.1009 Å.

Table IV. Secondary Equilibrium Isotope Effects (K_H/K_D) and Their Stretching (S) and Bending (B) Components for the General Process $CH_3Cl(CD_3Cl) \rightarrow CH_3^m(CD_3^m) + Cl^n$ (MP2/6-31+G* Calculations)

m	*n*	K_H/K_D	S	B
1	−1	2.02	0.93	2.17
0	0	2.72	0.84	3.24
−1	1	3.57	1.27	2.81

The bending vibrations summarized in Table III also differ. Focusing initially on the umbrella motion of the methyl group, the (unscaled) MP2/6-31+G* frequencies for CH_3Cl, CH_3^+, CH_3, and CH_3^- are, respectively, 1464, 1462, 482, and 819 cm^{-1}. The large difference between the cation and the radical reflects the very flat minimum of the latter. When all of the C–H bending frequencies are now taken into account, normal bending isotope effects are predicted generally for tetrahedral → trigonal processes, but a cation-forming process will have the smallest bending isotope effect, because of the minor role of the methyl umbrella motion.

The foregoing remarks can be placed on a quantitative basis by consideration of eqs 3a–3c, whose equilibrium constants are the *equilibrium isotope effects*, K_H/K_D, for the different unimolecular C–Cl bond-breaking pathways of CH_3Cl. Table IV summarizes these isotope effects, computed at MP2/6-31+G*. They are all normal. The stretching component is inverse for eqs 3a and 3b, and normal for eq 3c. The bending components are normal, but smallest for eq 3a.

$$CH_3Cl + CD_3^+ \rightleftharpoons CD_3Cl + CH_3^+ \quad (3a)$$

$$CH_3Cl + CD_3 \rightleftharpoons CD_3Cl + CH_3 \quad (3b)$$

$$CH_3Cl + CD_3^- \rightleftharpoons CD_3Cl + CH_3^- \quad (3c)$$

It is important to emphasize that although we have thus computed a normal isotope effect for the S_N1 process, as is observed experimentally for this mechanism in solution,[22,25] our data refer to the *equilibrium* isotope effect. A kinetic isotope effect is not accessible for a gas-phase S_N1 process because the reverse reaction, recombination of the ions, has no barrier in this case,[26] and the ionic process will in any event be disfavored.

(23) Inverse kinetic isotope effects have recently been observed experimentally for gas-phase S_N2 reactions. See: Gronert, S.; Depuy, C. H.; Bierbaum, V. M. *J. Am. Chem. Soc.* **1991**, *113*, 4009. We thank Professor C. H. DePuy for preprints of this paper, and of ref 21, and for numerous interesting discussions.

(24) Halevi, E. A. *Prog. Phys. Org. Chem.* **1963**, *1*, 109.

(25) Shiner, V. J. In *Isotope Effects in Chemical Reactions*; Collins, C. J., Bowman, N. S., Eds.; Van Nostrand Reinhold: New York, 1970; Chapter 2.

(26) For studies of cation–anion recombination in solution, see, e.g.: Ritchie, C. D. *Can. J. Chem.* **1986**, *64*, 2239. Arnett, E. M.; Molter, K. *J. Phys. Chem.* **1986**, *90*, 383. Shaik, S. S. *J. Org. Chem.* **1987**, *52*, 1563.

Table V. Coupling between Various Internal Coordinates during the Process CH_3Y (R) → $X\cdots CH_3Y$ (C) → $(X\text{-}CH_3\text{-}Y)^-$ (TS) (X = Y = Cl) (MP2/6-31+G* Calculations)

nature of coupling	magnitude × 10^2 [a]		
	R	C	TS
r_{CY}–r_{CX}		0.57[b]	3.33[b]
r_{CY}–r_{CH}	0.43[b]	0.19[b]	−0.19[b]
r_{CY}–α_{HCY}	5.20[c]	5.26[c]	4.12[c]
r_{CX}–α_{HCY}		−0.10[c]	−4.12[c]
r_{CH}–α_{HCY}	−1.21[b]	−1.49[b]	−1.30[b]

[a] In atomic units. [b] For stretch–stretch interactions, 1 au = 2242 kcal mol^{-1} Å^{-2}. [c] For stretch–bend interactions, 1 au = 20.7 kcal mol^{-1} Å^{-1} deg^{-1}.

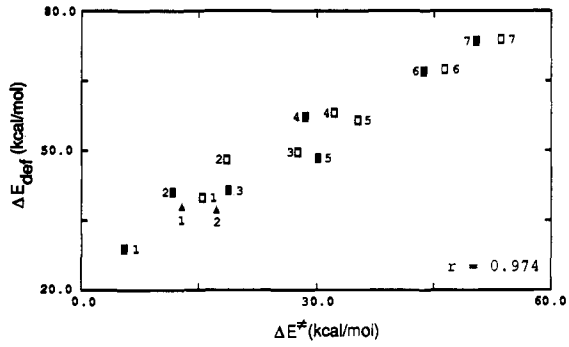

Figure 3. Relationship between $\Delta E^{\ddagger}$ and ΔE_{def} of identity methyl-transfer reactions as a function of the basis set and the nature of X: 4-31G, filled squares; 6-31+G*, open squares; MP2/6-31+G*, triangles. Points marked 1–7 refer respectively to (Cl, Cl), (F, F), (FO, OF), (CN, NC), (MeO, OMe), (NC, CN), and (HCC, CCH).

As discussed by Shaik and Pross,[4] the transition structure of a bimolecular identity methyl-transfer reaction $X_a^- + MeX_b$ can be described in terms of the valence bond configurations **1a**, **1b**, **2**, and **3**. Our tentative conclusion at this stage is that, with

$$[X_a{:}\,Me\cdot\cdot X_b] \qquad [X_a\cdot\cdot Me{:}X_b] \qquad [X_a\cdot Me{:}\cdot X_b]$$
$$\textbf{1a} \qquad\qquad \textbf{1b} \qquad\qquad \textbf{2}$$
$$[X_a{:}\,Me^+{:}X_b]$$
$$\textbf{3}$$

Cl^-/CH_3Cl as the prototype, analysis of the secondary kinetic isotope effect and its components points to **1** and **3** as the principal configurations, with **1** predominant. A predominance of **2** would have been signaled by a normal stretching contribution and, therefore, by a normal kinetic isotope effect; we believe that a predominance of **3** over **1** would have been signaled by a smaller change in the frequency of the umbrella motion of the methyl group than the change we calculate for C → TS (1414 → 1110 cm^{-1}). This tentative conclusion is consistent with the central feature of the Shaik–Pross description of the S_N2 mechanism, namely, that the barrier is the result of the movement of a *single* electron from X_a to X_b, coupled to molecular distortions along the reaction coordinate. The conclusion is also consistent with Shi and Boyd's recent charge analysis of the S_N2 transition structure.[6c]

Bürgi and Dunitz[27] and Kirby and Jones[28] have observed that variations in the geometrical parameters of a series of stable molecules of related structure parallel the energetics of bond-breaking processes involving these molecules. In this connection, it is instructive to examine the coupling between pairs of internal coordinates in R, C, and TS. This information can be found in the off-diagonal elements of the force constant matrices, and the data of interest are given in Table V for the process $X^- + CH_3Y \rightarrow XCH_3 + Y^-$ (X = Y = Cl). The meaning of positive coupling between two coordinates is that the energy increases as both coordinates are increased. In methyl chloride, the couplings between r_{CY} and α_{HCY}, and between r_{CY} and r_{CH}, are positive. Therefore, stretching of the C–Cl bond will be facilitated by a decrease in the H–C–Cl bond angle and also by a decrease in the

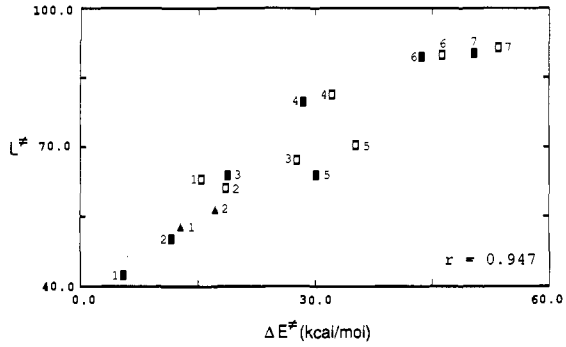

Figure 4. Relationship between $\Delta E^{\ddagger}$ and $L^{\ddagger}$ of identity methyl-transfer reactions as a function of the basis set and the nature of X. The identification of the points is the same as in Figure 3.

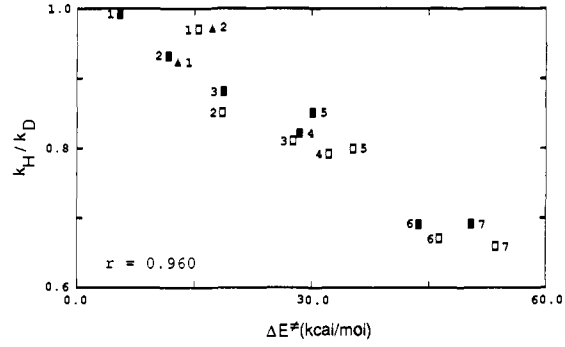

Figure 5. Variation in k_H/k_D and $\Delta E^{\ddagger}$ for the central barriers of identity methyl-transfer reactions as a function of the basis set and the nature of X. The identification of the points is the same as in Figure 3.

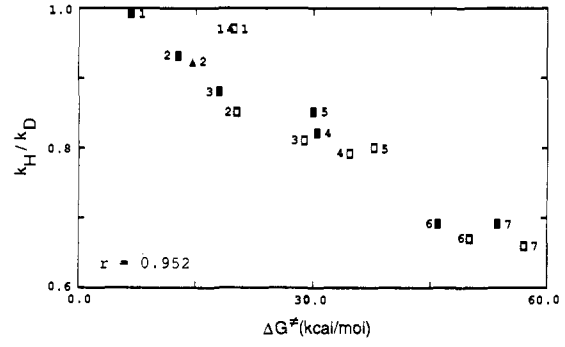

Figure 6. Variation in k_H/k_D and $\Delta G^{\ddagger}$ for the central barriers of identity methyl-transfer reactions as a function of the basis set and the nature of X. The identification of the points is the same as in Figure 3.

C–H bond length. The coupling between these latter quantities is negative: a decrease in the bond angle is facilitated by a decrease in the C–H bond length. In general, the signs of the coupling constants of Table V do not change with progress along the reaction coordinate,[27,28] The negative coupling between r_{CY} and r_{CH} in the TS is understandable: further extension of C–Y leads to product, and C–H also lengthens.

In the D_{3h} transition structure of an identity methyl-transfer reaction, α_{HCCl} is necessarily 90°. Because the coupling between r_{CX} and r_{CH} is an order of magnitude smaller than the other couplings shown in Table V, we might expect that since α_{HCY} does not vary with Y in the transition structures, neither does r_{CH}. This is indeed the case: The 4-31G C–H bond lengths of the D_{3h} structures (five examples) are 1.0585 ± 0.0003 Å; at 6-31+G* these bond lengths are 1.0610 ± 0.0004 Å (five examples); at

(27) Dunitz, J. D. *Philos. Trans. R. Soc. London, B* **1975**, *272*, 99. Bürgi, H. B.; Dunitz, J. D. *Acc. Chem. Res.* **1983**, *16*, 153. Bürgi, H. B.; Dunitz, J. D. *J. Am. Chem. Soc.* **1987**, *109*, 2924.

(28) Kirby, A. J.; Jones, P. G. *J. Am. Chem. Soc.* **1984**, *106*, 6207. Kirby, A. J. *Pure Appl. Chem.* **1987**, *59*, 1605.

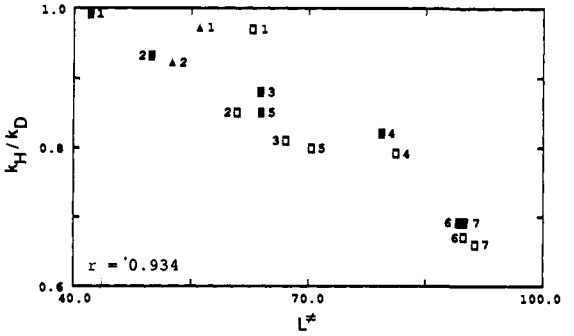

Figure 7. Relationship between k_H/k_D for the central barriers and looseness of the transition structures of identity methyl-transfer reactions as a function of the basis set and the nature of X. The identification of the points is the same as in Figure 3.

MP2/6-31+G* the bond lengths are 1.0732 ± 0.0008 Å (two examples). The implications of this finding are considered in the next section.

Trends in the Isotope Effects of Identity Reactions as X Is Varied. We now wish to relate the foregoing discussion to the trends in the energies, geometries, and isotope effects of gas-phase methyl-transfer reactions as the entering and leaving groups are varied. For the identity reactions of Tables I and II, the relationships among the various quantities are presented as Figures 3–7. In each of these figures, filled squares refer to 4-31G data, open squares to 6-31+G* data, and triangles to MP2/6-31+G* data. The r values shown in the figures are obtained with the assumption that all data points are linearly related.

Figures 3 and 4 show that the linear relationships between $\Delta E^{\ddagger}$ and ΔE_{def}, and between $\Delta E^{\ddagger}$ and $L^{\ddagger}$, are not basis set dependent. Both ΔE_{def} and $L^{\ddagger}$ increase as the barrier increases.[1] Figures 5 and 6 show the variation in the secondary kinetic isotope effect for the central barrier (C → TS) as a function of $\Delta E^{\ddagger}$, and also as a function of $\Delta G^{\ddagger}$. It is evident that the isotope effect decreases (becomes more inverse) as the barrier increases. Since $L^{\ddagger}$ *increases* as the barrier increases (Figure 4), it follows that k_H/k_D and $L^{\ddagger}$ vary inversely. This relationship is presented in Figure 7, which requires the conclusion that *secondary H/D isotope effects in identity methyl-transfer reactions decrease with increasing looseness of the transition structure.*

The inverse isotope effects exhibited by identity methyl-transfer reactions are therefore caused by a tightening of the C–H bonds along the reaction coordinate, and this tightening increases as the transition structures become looser. Moreover, since the C–H bond lengths of $(X{-}CH_3{-}X)^-$ transition structures do not depend upon X, the variations in the isotope effects must originate in the different C–H bond lengths of the reactants. This point is explored in Table VI, which shows the variations in $\Delta G^{\ddagger}$, $L^{\ddagger}$, and r_{CH} of the ion··molecule complexes as X and the basis set are varied. At each computational level, both $L^{\ddagger}$ and r_{CH} increase as $\Delta G^{\ddagger}$ increases.

Table VI. Relationships between the C–H Bond Lengths in $X^-\cdots CH_3X$ Complexes and the $\Delta G^{\ddagger}$ and $L^{\ddagger}$ of Identity S_N2 Reactions $X^- + CH_3X \rightarrow XCH_3 + X^-$

basis set	X, X	C–H bond length	$\Delta G^{\ddagger}$	$L^{\ddagger}$
4-31G	Cl, Cl	1.066	6.73	42.2
	F, F	1.068	12.76	50.0
	CN, NC	1.075	30.52	79.5
	NC, CN	1.078	46.00	89.2
	HCC, CCH	1.079	53.69	90.0
6-31+G*	Cl, Cl	1.073	19.91	62.9
	F, F	1.074	20.24	60.8
	CN, NC	1.077	34.67	81.3
	NC, CN	1.080	50.06	89.8
	HCC, CCH	1.081	57.02	91.2
MP2/6-31+G*	F, F	1.084	14.63	52.6
	Cl, Cl	1.085	19.37	56.1

Concluding Remarks

It appears that the commonly accepted view of the origins of secondary H/D kinetic isotope effects in methyl-transfer reactions is not valid, and that trends in these isotope effects are determined ultimately by trends in the C–H bond lengths of the reacting molecules. Although our results refer to the gas phase, and mainly to identity reactions, it will probably be necessary to rethink the current interpretation[10] of the isotope effects that are observed experimentally in the formation of an enzyme–substrate complex and in a nonidentity enzymatic methyl-transfer reaction. As a first step, we plan to extend the present work to a series of nonidentity methyl-transfer reactions. It is noteworthy that the nonidentity reaction involving F^- and Cl^- as the entering and leaving groups exhibits (Table II) an inverse k_H/k_D in the exoergic direction ($F^- + CH_3Cl$) ($\Delta G^{\ddagger}$ = 4.2 kcal/mol), and a normal k_H/k_D in the endoergic direction ($Cl^- + CH_3F$) ($\Delta G^{\ddagger}$ = 41.8 kcal/mol). For this one example, the behavior is opposite to that seen in Figure 6, but consistent with Schowen's finding that k_H/k_D decreases as the barrier decreases. In a recent study of the catalysis of methyl-transfer reactions by a cyclophane host (k_{cat}/k_{uncat} = 10^2),[29] Dougherty and his co-workers concluded that transition states are more polarizable and more tightly bound by the host than are ground states. How this effect influences the transition structure is not clear, but it would be desirable to know whether the catalysis observed by these researchers is accompanied by a decrease in k_H/k_D.

Acknowledgment. We thank the Natural Sciences and Engineering Research Council of Canada for financial support, and Simon Fraser University for generous allocation of computing resources. Many helpful discussions with Professor E. A. Halevi are also gratefully acknowledged.

Registry No. CH_3F, 593-53-3; CH_3Cl, 74-87-3; CH_3OF, 36336-08-0; CH_3CN, 75-05-8; CH_3OMe, 115-10-6; $CNCH_3$, 593-75-9; CH_3CCH, 74-99-7; D, 7782-39-0.

(29) Staufer, D. A.; Barrans, R. E., Jr.; Dougherty, D. A. *Angew. Chem., Int. Ed. Engl.* **1990**, *29*, 915.